

Molecular-Resolution Interrogation of a Porphyrin Monolayer by Ultrahigh Vacuum Tip-Enhanced Raman and Fluorescence Spectroscopy

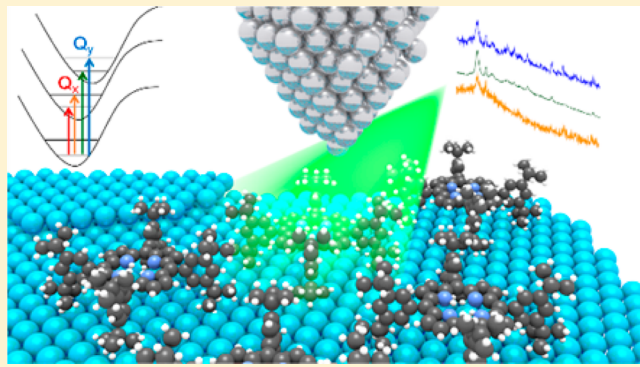
Naihao Chiang,[†] Nan Jiang,^{*,‡} Dhabih V. Chulhai,[†] Eric A. Pozzi,[‡] Mark C. Hersam,^{‡,§} Lasse Jensen,[†] Tamar Seideman,^{*,‡} and Richard P. Van Duyne^{*,†,‡}

[†]Applied Physics Graduate Program, [‡]Department of Chemistry, and [§]Department of Materials Science and Engineering, Northwestern University, Evanston, Illinois 60208, United States

[†]Department of Chemistry, The Pennsylvania State University, University Park, Pennsylvania 16802, United States

S Supporting Information

ABSTRACT: Tip-enhanced Raman scattering (TERS) and optically excited tip-enhanced fluorescence (TEF) of a self-assembled porphyrin monolayer on Ag(111) are studied using an ultrahigh vacuum scanning tunneling microscope (UHV-STM). Through selectively exciting different Q-bands of meso-tetrakis-(3,5-ditertiarybutylphenyl)-porphyrin (H_2TBPP), chemical information regarding different vibronic excited states is revealed by a combination of theory and experiment; namely, TERS and time-dependent density functional theory (TDDFT) simulations. The observed TEF spectra suggest a weak coupling of H_2TBPP to the substrate due to the bulky t-butyl groups and a possible alternative excited state decay path. This work demonstrates the potential of combining TERS and TEF for studying surface-mounted porphyrins on substrates, thus providing insight into porphyrin-sensitized solar cells and catalysis.



KEYWORDS: *tip-enhanced Raman spectroscopy (TERS), tip-enhanced fluorescence (TEF), ultrahigh vacuum scanning tunneling microscopy (UHV-STM), time-dependent density functional theory (TDDFT)*

Porphyrins are of great interest in the fields of chemistry, physics, biology, and medicine due to their natural abundance and distinct electronic, photonic, and catalytic properties.¹ Ordered porphyrin adlayers formed by self-assembly have been extensively investigated in the past.^{2–7} The most widely used technique for studying such self-assembled porphyrin systems is scanning tunneling microscopy (STM),^{5–9} with more recent emphasis placed on experiments done under ultrahigh vacuum (UHV) conditions.^{10–13} However, STM alone is insufficient at revealing much of the rich chemical information on these systems. A combination of optical spectroscopy and STM allows one to overcome this limitation.

In particular, *in situ* fluorescence of organic molecules adsorbed on metal substrates can be studied by STM-induced luminescence (STML).^{14,15} STML has been demonstrated to have single-molecule resolution^{16,17} due to the highly confined nanocavity plasmon generated by tunneling electrons inside STM junctions.^{18,19} The characteristic Q-band emissions of metal-free porphyrin adlayers were studied by electron excitation STML on noble metals,^{18,20–22} and on monolayer graphene²³ in a vacuum environment. In contrast, the photoluminescence (PL) of porphyrin adlayers has rarely

been explored because the metal surface strongly quenches fluorescence.

Raman scattering is an alternative spectroscopic technique using photon excitation, which is capable of studying vibrational, rotational, and other low-frequency modes of molecules. The introduction and subsequent growth of surface-enhanced Raman spectroscopy (SERS) has helped scientists overcome the detection related issue of low Raman cross-sections for organic molecules.^{24,25} In SERS, the incident and Raman scattered light is amplified by the localized surface plasmon resonance (LSPR) supported on nanostructured noble metal substrates. Amplification occurs through large enhancements to the electromagnetic (EM) fields²⁶ that are capable of reaching single-molecule sensitivity under favorable circumstances.^{27–29}

Similarly, Raman scattering from only a few molecules on a surface can be enhanced by a highly confined EM field created by optically exciting the LSPR of the tip–sample junction in an STM, or an atomic force microscope (AFM), with plasmoni-

Received: March 30, 2015

Revised: April 27, 2015

cally active noble metal tips.^{29,30} This technique is known as tip-enhanced Raman scattering (TERS).^{31,32} UHV and low-temperature environments have also been incorporated into TERS to increase the stability of molecules and to obtain spectra with higher signal-to-noise ratios.^{31,33–35} Recent advances in TERS have shown the capability of single-molecule imaging³⁵ as well as improving spatial resolution below 5 nm.^{36,37} For example, Dong, Hou, and co-workers have reported an impressive subnanometer TERS image of a single molecule.³⁸ Recent theoretical results suggest that quantum tunneling can modify the LSPR profile in gaps smaller than 1 nm,^{39,40} such as in STM, and may be partially responsible for such high spatial resolution. In addition, the richness of the chemical information provided by TERS reaches far beyond its high-resolution imaging ability.

Herein, we present a series of TERS spectra, recorded under UHV conditions, of a self-assembled *meso*-tetrakis(3,5-di-*t*-butylphenyl)- porphyrin (H_2 TBPP) monolayer grown on a single crystal Ag(111) surface. Excitation wavelengths were chosen to coincide as closely as possible with the different Q-band vibronic transition energies. The spectroscopic differences in the obtained TERS spectra are explained by time-dependent density functional theory (TDDFT), simulated resonance Raman spectra (RRS), and surface-enhanced resonance Raman scattering (SERRS) resulting from these different vibronic transitions. In addition, a series of tip-enhanced fluorescence (TEF) spectra with laser excitations in the Q-band region are shown to have a higher signal-to-noise ratio than those collected with tunneling electron excited STML.

The single crystal Ag(111) sample (Princeton Scientific Corp., one side polished <0.03 μ m) was cleaned by repeated cycles of Ar^+ ion sputtering and annealing at 750 K. H_2 TBPP molecules (Frontier Scientific) were thermally sublimed in UHV at 575 K onto the clean Ag(111) substrate. Electrochemically etched Ag tips⁴¹ were cleaned in UHV by Ar^+ ion sputtering before all experiments.

The system for obtaining UHV-TERS and -TEF has been described elsewhere.^{33,34} The experiments were performed at a base pressure of $\sim 2 \times 10^{-11}$ Torr.⁴² The pressure was monitored by a cold cathode gauge, and there was no change observed during both TERS and TEF experiments. Five different lasers: 514.5 nm continuous-wave (CW) Ar^+ ion laser (Spectra-Physics BeamLok 2026), 532 nm CW laser (Spectra-Physics Excelsior), 561 nm CW laser (LASOS DPSSL), 594 nm CW laser (Spectra-Physics Excelsior), and 632.8 nm HeNe laser (Research Electro optics) were used as excitation sources. The optical path was modified to fiber-couple to the Ar^+ ion laser. The silica Raman light generated from the fiber was removed by an interference filter (Semrock LL01-514-12.5). A laser power stabilizer (Brockton Electro-Optics Corp.) was used to stabilize the excitation power of all wavelengths at 1.00 mW (measured by the power stabilizer). The excitation polarization was rotated by a half-wave plate to be parallel to the tip axis. The laser beam was then expanded to ~ 25 mm in diameter and focused at the tip-sample junction at an angle of incidence of roughly 75° with respect to the Ag(111) surface normal. The Raman scattered light was collected at roughly the same angle through a viewport on the opposite side of the chamber, which was then focused onto a 100 μ m slit of an imaging spectrograph (Princeton Instrument SCT 320) equipped with a thermoelectrically cooled charge-coupled device (CCD) (Princeton Instrument PIXIS 400BR). TERS spectra were collected by a 1200 grooves/mm grating

blazed at 500 nm for 514.5, 532, 561, and 594 nm excitations. TEF and STML spectra were recorded by a 600 grooves/mm grating blazed at 750 nm. All power reported was measured by the power stabilizer, although 38% of the incident power was expected to be absorbed by both the sapphire windows and UHV viewport glass. The observed TERS and TEF intensities were recorded in analog-to-digital unit (ADU) since readings from a CCD were not absolute counts of photons. Four different tips were used in this study. The tips were switched for several different reasons: unexpected tip crashes, tip contaminated during the experiments, or decrease in TERS signal after sputtering. Same tips were used for both TERS and TEF experiments.

An excitation-wavelength-optimized silver film over nanosphere (AgFON) substrate⁴³ was used for obtaining H_2 TBPP SERRS reference spectra at 532 nm excitation. The AgFON was prepared by drop-coating 390 nm silica microspheres (Bangs Laboratories) on a polished Si wafer (MEMC Electronics). The nanospheres were then manually distributed evenly on the silicon surface. Silver films (200 nm thick) were deposited onto the nanosphere-covered Si wafer using a custom thermal evaporation system. The SERRS and PL spectra were measured in an inverted microscope (Nikon Eclipse Ti) system with a 20× microscope objective. Absorbance of H_2 TBPP in ethanol (2.5×10^{-6} M) was measured by a double beam spectrophotometer (Cary 5000).

The optimized geometry and normal modes of H_2 TBPP were obtained with the B3LYP/6-311G* level of theory using NWChem.^{44,45} Vibrational frequencies were scaled by a factor of 0.98 to account for missing anharmonicity in the simulations. The resonance Raman scattering of H_2 TBPP was simulated using a time-dependent wave packet formalism.⁴⁶ The Franck–Condon factors and the transition dipole derivatives (needed for the Herzberg–Teller contributions) were obtained from three-point numerical differentiation of the excited states energies and transition dipoles, respectively, along mass-weighted normal mode coordinates. The excited states lifetime parameters for a high-temperature Brownian oscillator solvent model^{47,48} were optimized to best match the solution-phase absorption spectrum. All simulated Raman spectra were broadened by Lorentzians with full width at half maxima of 7.0 cm^{-1} .

The dressed-polarizability formalism^{49,50} was used to simulate SERRS, where the molecular polarizabilities are dressed as

$$\alpha_{\alpha\beta}^{D,(k)} = \mathbf{E}_{loc,\gamma}^\alpha(\omega_s)\alpha_{\gamma\delta}^{(k)}(k)\mathbf{E}_{loc,\delta}^\beta(\omega_L) \quad (1)$$

where $\alpha^{(k)}$ is the polarizability for normal mode k , and \mathbf{E}_{loc} represents the local field enhancement matrices at the incident (ω_L) and scattered (ω_s) frequencies. These matrices generally depend on the orientation of the molecule with respect to the surface. However, on the basis of the STM images (Figure 1), results for parallel orientations (porphyrin rings parallel to the surface) better represent the experiments.

H_2 TBPP has a molecular structure containing a planar porphyrin ring with four 3,5-di-*t*-butylphenyl substituents at the meso carbon positions. The DFT-optimized geometry (Figure 1a) suggests that the plane of substituted phenyl rings is perpendicular to the plane of the center porphyrin ring. H_2 TBPP molecules were thermally evaporated onto a clean Ag(111) surface, which was maintained at room temperature (297 K). Similar to a previous study of copper phthalocya-

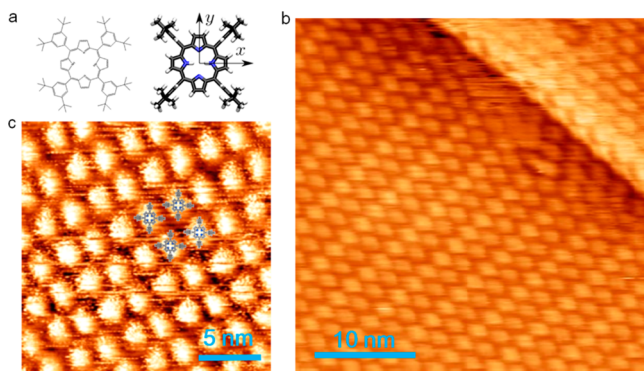


Figure 1. (a) Chemical structure and optimized geometry of H₂TBPP. (b) Large-scale STM topographic image ($35\text{ nm} \times 35\text{ nm}$) of an ordered H₂TBPP monolayer on a Ag(111) surface measured by a Ag tip (STM imaging condition: 1.00 V, 300 pA). (c) High-resolution STM image ($20\text{ nm} \times 20\text{ nm}$) of closed-packed H₂TBPP structure. Hard-sphere molecular model of H₂TBPP was inserted to indicate orientation of molecules. (STM imaging condition: 1.50 V, 100 pA).

nine,³³ individual H₂TBPP molecules cannot be observed by STM at low coverage. When the molecular coverage is close to a full monolayer, H₂TBPP self-assembles into a well-ordered adlayer, as shown in Figure 1, panel b. This observation results from the competition between molecule–molecule and molecule–substrate interactions.^{51,52} At room temperature, H₂TBPP molecules diffuse on open terraces of the Ag(111) surface, implying that individual molecules cannot be resolved at low coverage. This rapid diffusion further reveals that the interaction between H₂TBPP and Ag substrate is weak, as expected from the di-t-butylphenyl substituents. Only at approximately full monolayer coverage, surface diffusion of H₂TBPP molecules is strongly constrained by neighboring

molecules, and H₂TBPP–H₂TBPP interactions lead to the formation of an ordered structure.

While forming an ordered monolayer on a flat terrace, the H₂TBPP adlayer extends over several different step-edges of various heights. Hard-sphere molecular models of H₂TBPP were inserted into the high-resolution STM image shown in Figure 1, panel c, to indicate the orientation of H₂TBPP on Ag(111). The uniform self-assembled monolayer can be readily formed on metal substrates and thus presents a chemically uniform organic thin layer.

A typical porphyrin molecule exhibits multiple vibronic transitions in the near-UV and visible region. At 419 nm, H₂TBPP shows a strong transition to the third and fourth electronically excited states, known as the Soret band (data not shown). It also has four weak absorption bands peaks at 515, 549, 593, and 649 nm. These bands are denoted as Q_y(1,0), Q_y(0,0), Q_x(1,0), and Q_x(0,0), respectively, which indicate transitions to the two lowest electronic excited states (Figure 2a). The TDDFT-simulated absorption spectrum is in good agreement with the measured absorption in ethanol, with the only exception being the Q_y(1,0) band, which is slightly blue-shifted. The observed blue shift is likely due to Duschinsky rotations⁵³ or frequency anharmonicity,⁵⁴ absent in the theory used here. However, we cannot rule out solvent and surface effects or interactions with other molecules as possible sources for the observed discrepancy.

Figure 2, panel b shows a TERS spectrum with 532 nm CW excitation (1.00 mW). The tip–sample junction was maintained at 0.1 V and 500 pA while the TERS spectrum was acquired. This spectrum agrees with previously reported results³⁸ but shows more vibrational features due to improved signal-to-noise ratio. This improved ratio is a consequence of constructing all optics outside the STM chamber, which gives a UHV base pressure less than 5×10^{-11} Torr. All modes were

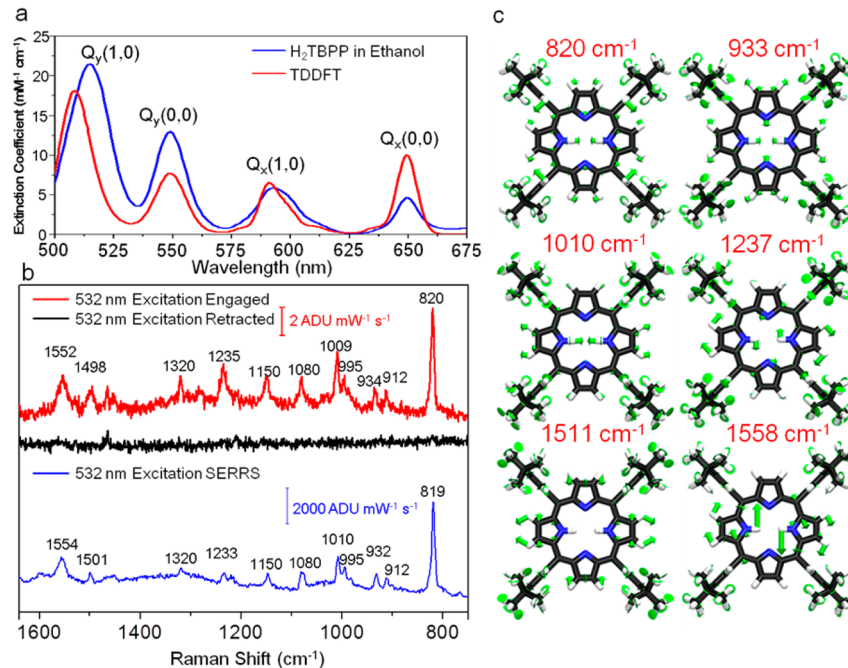


Figure 2. (a) Absorption spectrum of 2.5×10^{-6} M H₂TBPP in ethanol (blue) and TD-DFT calculated spectrum (red). (b) UHV-TERS tip-engaged (red) and tip-retracted (black) spectra of H₂TBPP monolayer on Ag(111) with 532 nm excitation (0.1 V, 500 pA, 180 s) and SERS spectrum of H₂TBPP adlayer on AgFON substrate with 532 nm excitation (10 s). (c) Selected TDDFT calculated Raman active normal modes of an H₂TBPP molecule.

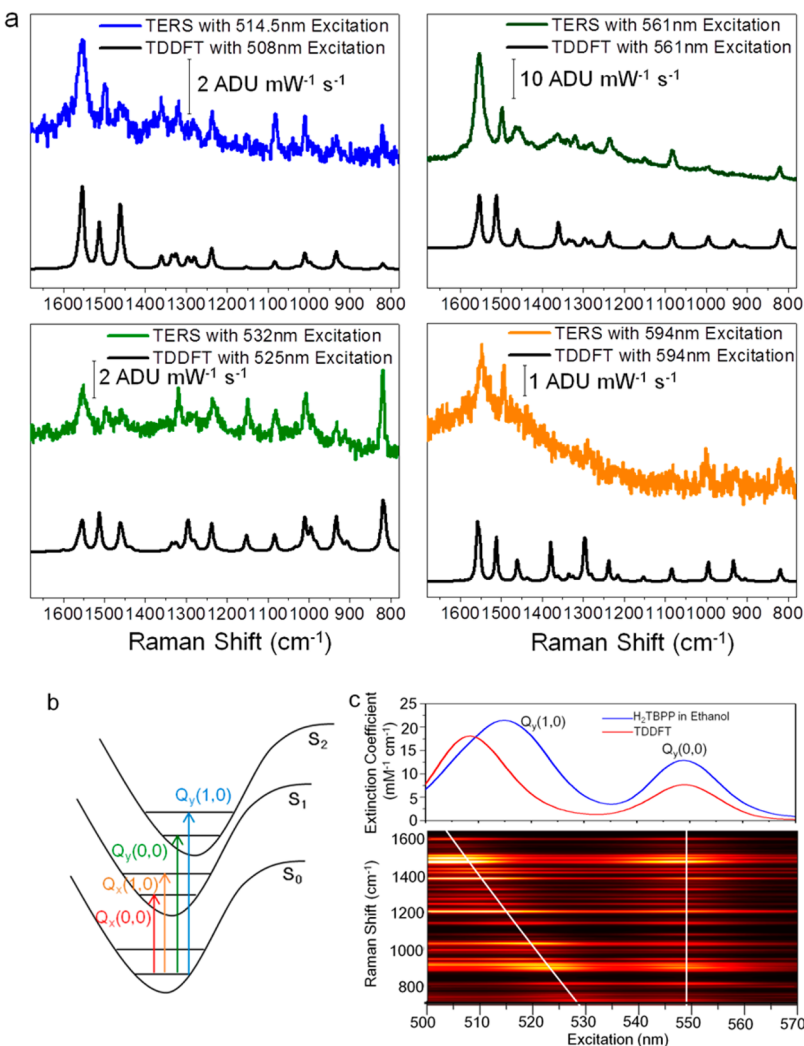


Figure 3. (a) UHV-TERS spectra of H₂TBPP adlayer on Ag(111) (tip-engaged spectra with tip-retracted spectra subtracted) with 514.5, 532, 561, and 594 nm excitation, and the corresponding TDDFT simulations of plasmonically enhanced Raman spectra with polarization of the excitation parallel to the tip axis. (b) Schematics of the resonance Raman process of H₂TBPP. (c) TDDFT simulated excitation profile for resonance Raman spectra of H₂TBPP with excitation from 490–570 nm. The white lines are the corresponding Q_y(1,0) and Q_y(0,0) excitation energies for each vibrational mode.

correlated with those observed in the reference SERRS spectrum that was recorded with the identical excitation wavelength. The tip-retracted spectrum shows no far-field scattering, demonstrating the necessary condition for the Ag probe not being contaminated by the analytes from the sample. A selection of normal modes with strong TERS/SERRS intensities are shown in Figure 2, panel c (more modes are shown in Supporting Information S1). As expected from the C_{2v} symmetry of H₂TBPP, the in-plane skeletal porphyrin modes are more intense in both the observed TERS and SERRS spectra.

To further investigate the TERS spectra of H₂TBPP, four distinct excitation wavelengths were used to selectively pump the different Q-bands: 514.5 nm excitation for the Q_y(1,0) band, 561 nm excitation for the Q_y(0,0) band, 594 nm excitation for the Q_x(1,0) band, and 633 nm excitation for the Q_x(0,0) band. All TERS spectra were recorded with 1.00 mW incident laser power and an acquisition time of 180 s. Different STM bias voltages were used for obtaining TERS spectra with the best signal-to-noise ratios, while the STM was held in constant tunneling current mode with a set-point of 300 pA.

We note that there is no reproducible STM bias-dependence in the TERS signal intensity.

Figure 3, panel a shows a series of TERS spectra using different excitation wavelengths with corresponding TDDFT calculated spectra. We account for the blue shift of the Q_y(1,0) transition in the TDDFT-simulated absorption spectrum (Figure 2a) by shifting the excitation wavelengths in the TDDFT-simulated SERRS, thereby retaining relative overlap with this band. Specifically, we used 508 and 525 nm as the excitation wavelengths in the TDDFT calculations to remain congruent with the experimental data acquired with 514.5 and 532 nm excitations, respectively. Table 1 shows the TDDFT calculated excited states properties, including the x- (μ_x^{0n}) and y- (μ_y^{0n}) components of the transition dipole moments, and the homogeneous broadening factor (Γ), used in the simulated resonance Raman and plasmonically enhanced Raman spectra.

The TERS spectra were similar for all excitations, except in the region from 1200–1400 cm⁻¹. Additionally, the 1010 cm⁻¹ Raman mode was stronger when exciting the Q_y(1,0) transition, while the 819 cm⁻¹ mode had the highest relative intensity when using 532 nm excitation. These spectral

Table 1. TDDFT Calculated Excited States Properties Used for the Simulation of the RRS and TERS of H₂TBPP

	ΔE used ^a (calc.) (eV)	μ_x^{On} (D)	μ_y^{On} (D)	Γ^a (cm ⁻¹)
$S_1(Q_x)$	1.9097 (2.1765)	1.0343	0.0021	120.0
$S_2(Q_x)$	2.2584 (2.3247)	-0.0009	1.1639	250.0
$S_3(B_x)$	3.0765 (3.1352)	-8.3296	-0.0097	700.0
$S_4(B_x)$	2.9591 (3.2539)	-0.0130	10.5358	300.0

^aThe values of ΔE and Γ used best reproduced experimental data. For the high-temperature Brownian oscillator solvent model, a value of $\kappa = 0.1$ was used for all states.

differences are explained by the theory of resonance Raman spectroscopy as follows. For the Q(0,0) bands (561 and 594 nm excitation), H₂TBPP molecules were excited to the ground vibrational state ($v = 0$) of the corresponding electronically excited states, S_1 for the Q_x transitions and S_2 for the Q_y transitions, as indicated in Figure 3, panel b. For the Q(1,0) transitions, the molecules were also excited to the first vibrational excited state of a specific normal mode in that electronic excited state. A top-down waterfall plot (Figure 3c) shows a TDDFT-simulated resonance Raman excitation profile in the region of the $Q_y(1,0)$ and the $Q_x(0,0)$ transitions. The figure shows that each normal mode has a maximum at the $Q_y(0,0)$ excitation (~550 nm) and another maximum at the $Q_y(0,0)$ energy plus the energy of the corresponding $v = 1$ state. In our experimental results, the 532 nm excitation (525 nm in TDDFT calculation) is closer to the $v = 1$ resonance of the 819 cm⁻¹ mode, while the 514.5 nm excitation (508 nm in TDDFT calculation) is in better resonance with $v = 1$ for the 1554 cm⁻¹ mode. All tip-engaged and tip-retracted spectra are shown in the Supporting Information S2.

TERS with 633 nm excitation, in resonance with the $Q_x(0,0)$ band, was not observed since the fingerprint spectral region of the Raman signal was covered by the strong fluorescence of

H₂TBPP, which will be further discussed later. However, TDDFT simulated Raman excitation profile in the Q_x region (Supporting Information S3) shows similar behavior as in the Q_y region.

Figure 4, panel a shows a series of TEF spectra, tip-engaged minus tip-retracted, with excitation at the different Q-bands. All TEF spectra were acquired under STM conditions of 1.0 V and 300 pA to avoid contributions of signal from STML. There is no fluorescence observed without laser excitation. This indicates that the STM condition used for the TEF experiments was insufficient to excite STML. We also note that there was no far-field fluorescence recorded in any of the tip-retracted spectra (Supporting Information S4). Therefore, the 1.00 mW laser excitation was also not sufficient to initiate an observable fluorescence signal from monolayer H₂TBPP in the absence of tip enhancement. To excite the fluorescence by tunneling electrons only, both a higher bias voltage and tunneling current are required. At 2.5 V and 1000 pA, a strong increase in STML signal was observed (Figure 4b). This was consistent with previously reported results.^{55,56} The 655 and 720 nm fluorescence peaks are assigned to the Q(0,0) and Q(0,1) transitions, respectively.

When the system is excited at 633 nm, near the $Q_x(0,0)$ transition, the relative intensities of the two emitted fluorescence peaks were different than those excited at other Q-bands. Similar excitation wavelength dependence of fluorescence was reported for other porphyrins, and a dual emission process originating from the tautomerism of metal free porphyrins was proposed to explain such phenomena.⁵⁷

Fluorescence is known to be quenched near a flat metal surface,⁵⁵ with the distance dependence of the nonradiative excited state decay rate proportional to d^{-4} , where d represents the distance between the surface and the plane of the porphyrin ring.⁵⁸ By using a hard-sphere model of a DFT-optimized H₂TBPP molecule on an atomically flat Ag(111) surface

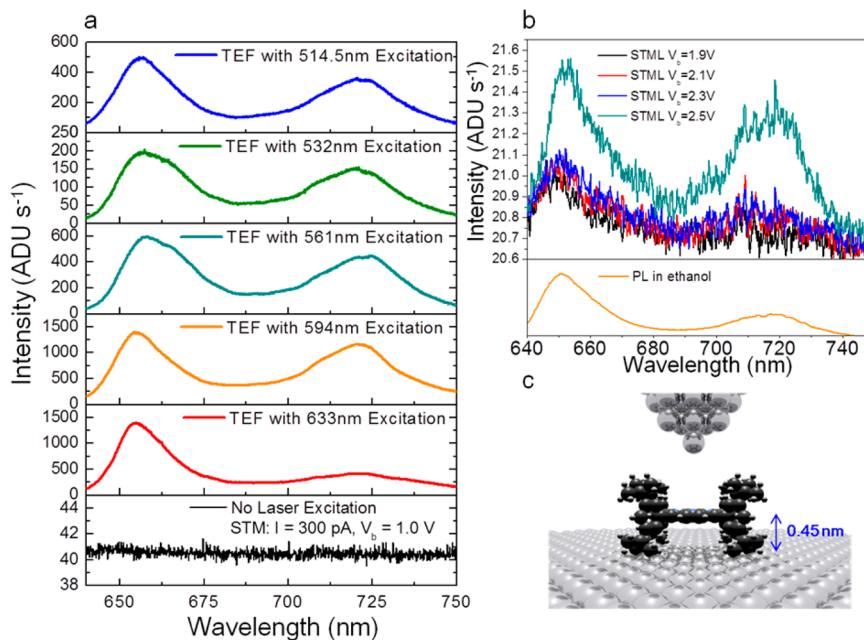


Figure 4. (a) UHV-TEF spectra of a H₂TBPP adlayer on Ag(111) (tip-engaged spectra with tip-retracted spectra subtracted) with 514.5, 532, 561, 594, and 633 nm excitation (1.00 mW) (STM conditions: 1.0 V, 300 pA). (b) STML spectra of H₂TBPP adlayer on Ag(111) as a function of STM bias voltages (STM tunneling current: 1.0 nA) and a reference PL spectra of 2.5 × 10⁻⁶ M H₂TBPP in ethanol (532 nm, 4.0 μW). (c) Schematic of an optimized H₂TBPP molecule adsorbed on the Ag(111) surface.

(Figure 4c), we estimate that the t-butylphenyl groups lift the center porphyrin ring by approximately 0.45 nm away from the Ag surface.

Conversely, enhancement of optical processes is stronger when the affected molecules are closer to a plasmonic material. The enhancement factor (EF_{flu}) of TEF due to a noble metal tip is given by⁵⁹

$$EF_{flu} \approx |E|^2 \left(\frac{q}{q^0} \right) \quad (2)$$

where E is the local electric field enhancement factor, and q and q^0 are the quantum yield of the emission with and without local field enhancement, respectively. Recent theoretical works by Nitzan and co-workers suggested that q should reflect the total system dipole, which includes the molecular dipole and the dipole induced on the particle, and hence demonstrated higher q when the molecular frequency is close to the plasmonic resonance.⁶⁰ By incorporating this effect into eq 2, the fluorescence enhancement, EF_{flu} , is expected to be greater than $|E|^2$. Therefore, the observations of TEF are likely due to a combination of lower nonradiative energy transfer to the substrate with increasing separation of the porphyrin ring from the surface and high enhancement of fluorescence by the plasmonic tip.

In this study, both UHV-TERS and UHV-TEF spectra of monolayer self-assembled H₂TBPP on a Ag(111) surface with excitation covering different Q-bands are reported. The spectroscopic difference in TERS due to excitation to different vibronic excited states was explained by TDDFT simulated (SE)RRS. The unexpected observation of TEF spectra is attributed to weak coupling of the molecular adlayer to the metal substrate combining with the effect of high signal enhancement by the plasmonic tip. The radiative emission is amplified without sacrificing much due to the nonradiative decay of the whole system. The wavelength-dependent TEF might hint at an alternative radiative decay path for the excited state of H₂TBPP on metal substrates. The combination of STM and optical spectroscopy was shown to provide a powerful probe of chemical properties. Future application of these techniques to other important research areas involving porphyrins, such as porphyrin-sensitized solar cells, photodynamic therapy, and the design of nanomaterials and nanodevices can be envisioned.

ASSOCIATED CONTENT

Supporting Information

More TDDFT calculated Raman active normal modes of an H₂TBPP molecule, all near-field and far-field spectra for UHV-TERS, TDDFT simulation of Raman excitation profile in the Q_x region, and near-field and far-field spectra for UHV-TEF. The Supporting Information is available free of charge on the ACS Publications website at DOI: 10.1021/acs.nanolett.5b01225.

AUTHOR INFORMATION

Corresponding Authors

*E-mail: n-jiang@northwestern.edu.

*E-mail: vanduyne@northwestern.edu.

Notes

The authors declare no competing financial interest.

ACKNOWLEDGMENTS

Primary support for this work was provided by the Department of Energy Office of Basic Energy Sciences (SISGR Grant DE-FG02-09ER16109) and the National Science Foundation Center for Chemical Innovation on Chemistry at the Space-Time Limit (Grant CHE-1414466). Additional support for facilities and instrumentation was provided by the National Science Foundation Materials Research Science and Engineering Center (Grant DMR-1121262). E.A.P. acknowledges support from the National Science Foundation Graduate Research Fellowship under Grant DGE-1324585. The authors also thank Dr. Nathan Greenelch, Dr. Jordan Klingsporn, Dr. Guillaume Goubert, and Prof. Matthew Sonntag for helpful discussions. Furthermore, L.J. and D.V.C. acknowledge support received from Research Computing and Cyberinfrastructure, a unit of Information Technology Services at Penn State.

REFERENCES

- (1) Auwärter, W.; Écija, D.; Klappenberger, F.; Barth, J. V. *Nat. Chem.* **2015**, 7 (2), 105–120.
- (2) Barlow, D. E.; Scudiero, L.; Hipps, K. W. *Langmuir* **2004**, 20 (11), 4413–4421.
- (3) Buchner, F.; Schwald, V.; Comanici, K.; Steinrück, H.-P.; Marbach, H. *ChemPhysChem* **2007**, 8 (2), 241–243.
- (4) Qiu, X.; Wang, C.; Zeng, Q.; Xu, B.; Yin, S.; Wang, H.; Xu, S.; Bai, C. *J. Am. Chem. Soc.* **2000**, 122 (23), 5550–5556.
- (5) Scudiero, L.; Barlow, D. E.; Mazur, U.; Hipps, K. W. *J. Am. Chem. Soc.* **2001**, 123 (17), 4073–4080.
- (6) Suto, K.; Yoshimoto, S.; Itaya, K. *J. Am. Chem. Soc.* **2003**, 125 (49), 14976–14977.
- (7) Yokoyama, T.; Yokoyama, S.; Kamikado, T.; Okuno, Y.; Mashiko, S. *Nature* **2001**, 413 (6856), 619–621.
- (8) Joshi, S.; Bischoff, F.; Koitz, R.; Ecija, D.; Seufert, K.; Seitsonen, A. P.; Hutter, J.; Diller, K.; Urgel, J. I.; Sachdev, H.; Barth, J. V.; Auwärter, W. *ACS Nano* **2013**, 8 (1), 430–442.
- (9) Phan, T. H.; Wandelt, K. *Surf. Sci.* **2013**, 607 (0), 82–91.
- (10) Heim, D.; Écija, D.; Seufert, K.; Auwärter, W.; Aurisicchio, C.; Fabbro, C.; Bonifazi, D.; Barth, J. V. *J. Am. Chem. Soc.* **2010**, 132 (19), 6783–6790.
- (11) Yang, Y.; Wang, C. *Chem. Soc. Rev.* **2009**, 38 (9), 2576–2589.
- (12) Kudernac, T.; Lei, S.; Elemans, J. A. A. W.; De Feyter, S. *Chem. Soc. Rev.* **2009**, 38 (2), 402–421.
- (13) Sedona, F.; Di Marino, M.; Basagni, A.; Colazzo, L.; Sambi, M. *J. Phys. Chem. C* **2013**, 118 (3), 1587–1593.
- (14) Berndt, R.; Gimzewski, J. K.; Johansson, P. *Phys. Rev. Lett.* **1991**, 67 (27), 5.
- (15) Gimzewski, J. K.; Reihl, B.; Coombs, J. H.; Schlittler, R. R. *Z. Phys. B: Condens. Matter* **1988**, 72 (4), 497–501.
- (16) Qiu, X. H.; Nazin, G. V.; Ho, W. *Science* **2003**, 299 (5606), 542–546.
- (17) Berndt, R.; Gaisch, R.; Gimzewski, J. K.; Reihl, B.; Schlittler, R. R.; Schneider, W. D.; Tschudy, M. *Science* **1993**, 262 (5138), 1425–1427.
- (18) Dong, Z. C.; Zhang, X. L.; Gao, H. Y.; Luo, Y.; Zhang, C.; Chen, L. G.; Zhang, R.; Tao, X.; Zhang, Y.; Yang, J. L.; Hou, J. G. *Nat. Photonics* **2010**, 4 (1), 50–54.
- (19) Le Ru, E. C.; Etchegoin, P. G.; Grand, J.; Félidj, N.; Aubard, J.; Lévi, G. *J. Phys. Chem. C* **2007**, 111 (44), 16076–16079.
- (20) Nishitani, R.; Liu, H.; Iwasaki, H. *Appl. Phys. Lett.* **2012**, 100, 051102.
- (21) Hongwen, L.; Ryusuke, N.; Yutaka, I.; Tatsuo, Y.; Yoshio, A.; Hiroshi, I. *Jpn. J. Appl. Phys.* **2005**, 44 (4L), L566.
- (22) Liu, H. W.; Nishitani, R.; Han, T. Z.; Ie, Y.; Aso, Y.; Iwasaki, H. *Phys. Rev. B* **2009**, 79 (12), 125415.
- (23) Geng, F.; Kuang, Y.; Yu, Y.; Liao, Y.; Zhang, Y.; Zhang, Y.; Dong, Z. *J. Lumin.* **2015**, 157 (0), 39–45.

- (24) Stiles, P. L.; Dieringer, J. A.; Shah, N. C.; Van Duyne, R. P. *Ann. Rev. Anal. Chem.* **2008**, *1* (1), 601–626.
- (25) Jeanmaire, D. L.; Van Duyne, R. P. *J. Electroanal. Chem. Interfacial Electrochem.* **1977**, *84* (1), 1–20.
- (26) Hao, E.; Schatz, G. C. *J. Chem. Phys.* **2004**, *120* (1), 357–366.
- (27) Kneipp, K.; Wang, Y.; Kneipp, H.; Perelman, L.; Itzkan, I.; Dasari, R.; Feld, M. *Phys. Rev. Lett.* **1997**, *78* (9), 1667–1670.
- (28) Dieringer, J. A.; Lettan, R. B.; Scheidt, K. A.; Van Duyne, R. P. *J. Am. Chem. Soc.* **2007**, *129* (51), 16249–16256.
- (29) Sonntag, M. D.; Klingsporn, J. M.; Garibay, L. K.; Roberts, J. M.; Dieringer, J. A.; Seideman, T.; Scheidt, K. A.; Jensen, L.; Schatz, G. C.; Van Duyne, R. P. *J. Phys. Chem. C* **2011**, *116* (1), 478–483.
- (30) Stöckle, R. M.; Suh, Y. D.; Deckert, V.; Zenobi, R. *Chem. Phys. Lett.* **2000**, *318* (1–3), 131–136.
- (31) Pozzi, E. A.; Sonntag, M. D.; Jiang, N.; Chiang, N.; Seideman, T.; Hersam, M. C.; Van Duyne, R. P. *J. Phys. Chem. Lett.* **2014**, *5* (15), 2657–2661.
- (32) Pozzi, E. A.; Sonntag, M. D.; Jiang, N.; Klingsporn, J. M.; Hersam, M. C.; Van Duyne, R. P. *ACS Nano* **2013**, *7* (2), 885–888.
- (33) Jiang, N.; Foley, E. T.; Klingsporn, J. M.; Sonntag, M. D.; Valley, N. A.; Dieringer, J. A.; Seideman, T.; Schatz, G. C.; Hersam, M. C.; Van Duyne, R. P. *Nano Lett.* **2011**, *12* (10), 5061–5067.
- (34) Klingsporn, J. M.; Jiang, N.; Pozzi, E. A.; Sonntag, M. D.; Chulhai, D.; Seideman, T.; Jensen, L.; Hersam, M. C.; Duyne, R. P. V. *J. Am. Chem. Soc.* **2014**, *136* (10), 3881–3887.
- (35) Steidtner, J.; Pettinger, B. *Phys. Rev. Lett.* **2008**, *100* (23), 236101.
- (36) Chen, C.; Hayazawa, N.; Kawata, S. *Nat. Commun.* **2014**, *5*.
- (37) Deckert-Gaudig, T.; Kämmer, E.; Deckert, V. *J. Biophotonics* **2012**, *5* (3), 215–219.
- (38) Zhang, R.; Zhang, Y.; Dong, Z. C.; Jiang, S.; Zhang, C.; Chen, L. G.; Zhang, L.; Liao, Y.; Aizpurua, J.; Luo, Y.; Yang, J. L.; Hou, J. G. *Nature* **2013**, *498* (7452), 82–86.
- (39) Esteban, R.; Borisov, A. G.; Nordlander, P.; Aizpurua, J. *Nat. Commun.* **2012**, *3*, 825.
- (40) Savage, K. J.; Hawkeye, M. M.; Esteban, R.; Borisov, A. G.; Aizpurua, J.; Baumberg, J. J. *Nature* **2012**, *491* (7425), 574–577.
- (41) Zhang, W.; Yeo, B. S.; Schmid, T.; Zenobi, R. *J. Phys. Chem. C* **2007**, *111* (4), 1733–1738.
- (42) Foley, E. T.; Yoder, N. L.; Guisinger, N. P.; Hersam, M. C. *Rev. Sci. Instrum.* **2004**, *75* (12), 5280–5287.
- (43) Greenelch, N. G.; Blaber, M. G.; Henry, A.-I.; Schatz, G. C.; Van Duyne, R. P. *Anal. Chem.* **2013**, *85* (4), 2297–2303.
- (44) Bylaska, E. J. *NWChem, A Computational Chemistry Package for Parallel Computers*, version 5.1.; Pacific Northwest National Laboratory: Richland, WA, 2007; pp 99352–0999.
- (45) Valiev, M.; Bylaska, E. J.; Govind, N.; Kowalski, K.; Straatsma, T. P.; Van Dam, H. J. J.; Wang, D.; Nieplocha, J.; Apra, E.; Windus, T. L.; de Jong, W. A. *Comput. Phys. Commun.* **2010**, *181* (9), 1477–1489.
- (46) Silverstein, D. W.; Jensen, L. *J. Chem. Phys.* **2012**, *136* (6), 064110.
- (47) Li, B.; Johnson, A. E.; Mukamel, S.; Myers, A. B. *J. Am. Chem. Soc.* **1994**, *116* (24), 11039–11047.
- (48) Myers, A. B. *Annu. Rev. Phys. Chem.* **1998**, *49* (1), 267–295.
- (49) Chulhai, D. V.; Jensen, L. *J. Phys. Chem. C* **2013**, *117* (38), 19622–19631.
- (50) Janesko, B. G.; Scuseria, G. E. *J. Chem. Phys.* **2006**, *125* (12), 124704.
- (51) Cheng, Z. H.; Gao, L.; Deng, Z. T.; Jiang, N.; Liu, Q.; Shi, D. X.; Du, S. X.; Guo, H. M.; Gao, H. J. *J. Phys. Chem. C* **2007**, *111* (26), 9240–9244.
- (52) Jiang, N.; Zhang, Y. Y.; Liu, Q.; Cheng, Z. H.; Deng, Z. T.; Du, S. X.; Gao, H. J.; Beck, M. J.; Pantelides, S. T. *Nano Lett.* **2010**, *10* (4), 1184–1188.
- (53) Yang, P.; Qi, D.; You, G.; Shen, W.; Li, M.; He, R. *J. Chem. Phys.* **2014**, *141* (12), 124304.
- (54) Yang, L.; Zhu, C.; Yu, J.; Lin, S. H. *Chem. Phys.* **2012**, *400* (0), 126–136.
- (55) Dong, Z. C.; Guo, X. L.; Trifonov, A.; Dorozhkin, P.; Miki, K.; Kimura, K.; Yokoyama, S.; Mashiko, S. *Phys. Rev. Lett.* **2004**, *92* (8), 086801.
- (56) Liu, H. W.; Ie, Y.; Nishitani, R.; Aso, Y.; Iwasaki, H. *Phys. Rev. B* **2007**, *75* (11), 115429.
- (57) Uttamlal, M.; Holmes-Smith, A. S. *Chem. Phys. Lett.* **2008**, *454* (4–6), 223–228.
- (58) Chance, R. R.; Prock, A.; Silbey, R. *Adv. Chem. Phys.* **1978**, *37* (1), 65.
- (59) Mauser, N.; Hartschuh, A. *Chem. Soc. Rev.* **2014**, *43* (4), 1248–1262.
- (60) Sukharev, M.; Freifeld, N.; Nitzan, A. *J. Phys. Chem. C* **2014**, *118* (20), 10545–10551.